J Neurophysiol. Author manuscript; available in PMC 2016 April 28.

Published in final edited form as:
J Neurophysiol. 2009 October ; 102(4): 2273–2287. doi:10.1152/jn.00282.2009.

SK Channels Gate Information Processing In Vivo by Regulating an Intrinsic Bursting Mechanism Seen In Vitro

Natalia Toporikova[1] and **Maurice J. Chacron**[1,2]

[1]Department of Physiology, Center for Nonlinear Dynamics, McGill University, Montreal, Quebec, Canada

[2]Department of Physics, McGill University, Montreal, Quebec, Canada

Abstract

Understanding the mechanistic substrates of neural computations that lead to behavior remains a fundamental problem in neuroscience. In particular, the contributions of intrinsic neural properties such as burst firing and dendritic morphology to the processing of behaviorally relevant sensory input have received much interest recently. Pyramidal cells within the electrosensory lateral line lobe of weakly electric fish display an intrinsic bursting mechanism that relies on somatodendritic interactions when recorded in vitro: backpropagating somatic action potentials trigger dendritic action potentials that lead to a depolarizing afterpotential (DAP) at the soma. We recorded intracellularly from these neurons in vivo and found firing patterns that were quite different from those seen in vitro: we found no evidence for DAPs as each somatic action potential was followed by a pronounced afterhyperpolarization (AHP). Calcium chelators injected in vivo reduced the AHP, thereby unmasking the DAP and inducing in vitro-like bursting in pyramidal cells. These bursting dynamics significantly reduced the cell's ability to encode the detailed time course of sensory input. We performed additional in vivo pharmacological manipulations and mathematical modeling to show that calcium influx through *N*-methyl-D-aspartate (NMDA) receptors activate dendritic small conductance (SK) calcium-activated potassium channels, which causes an AHP that counteracts the DAP and leads to early termination of the burst. Our results show that ion channels located in dendrites can have a profound influence on the processing of sensory input by neurons in vivo through the modulation of an intrinsic bursting mechanism.

INTRODUCTION

It was once thought that single neurons could be viewed as passive devices that sum up synaptic input and fire action potentials when this sum exceeds a given threshold. This traditional view has, however, been challenged over the last decades by studies showing that neurons possess active properties such as the firing of packets of action potentials followed by quiescence. This phenomenon, better known as burst firing, is ubiquitous within the CNS (Krahe and Gabbiani 2004). It has been found that burst firing can be elicited in vitro in many neurons, which has greatly facilitated the characterization of the ion channel

Address for reprint requests and other correspondence: M. J. Chacron, 3655 Sir William Osler, Rm. 1137, Montreal, Quebec H3G 1Y6, Canada, (maurice.chacron@mcgill.ca).

interactions that lead to bursting (Brumberg et al. 2000; Izhikevich 2000; Jung et al. 2001; Krahe and Gabbiani 2004; Wang and Rinzel 1995). A variety of functions have been proposed for burst firing such as feature detection (Gabbiani et al. 1996; Lesica and Stanley 2004; Lisman 1997; Metzner et al. 1998; Ritz and Sejnowski 1997) and gating of sensory information (Kim and McCormick 1998; Ramcharan et al. 2000; Sherman 2001). However, linking the packets of action potentials seen in vivo to burst firing seen in vitro has proven difficult because it is not known in general how in vivo conditions will affect burst firing seen in vitro. Studies exploiting well-characterized systems that are amenable to both in vitro and in vivo studies are necessary to understand the contributions of intrinsic firing dynamics such as bursting to neural computations that lead to behavior.

Gymnotiform weakly electric fish generate a quasi-sinusoidal electric organ discharge (EOD) that is distorted by objects with a conductivity different from that of the surrounding water (Turner et al. 1999). Electroreceptors on the fish's skin sense EOD amplitude modulations (AMs) caused by nearby objects (Bastian 1981) and synapse unto pyramidal cells within the electrosensory lateral line lobe (ELL) (Maler et al. 1991; Turner and Maler 1999). The responses of these pyramidal cells to sensory input have been well characterized in vivo (Bastian and Nguyenkim 2001; Chacron 2006; Chacron and Bastian 2008; Chacron et al. 2001b, 2003a, 2005c, 2007; Doiron et al. 2003a; Ellis et al. 2007a; Krahe et al. 2008). However, in vitro studies have shown that these cells display a well-characterized intrinsic burst mechanism that relies on a somatodendritic interaction (Lemon and Turner 2000; Turner et al. 1994).

We studied the bursting properties of ELL pyramidal cells in vivo via intracellular recordings and found significant differences with the firing patterns seen in vitro. Our experiments show that these differences can be explained the activation of dendritic SK1 channels by feedback input in vivo through calcium influx by *N*-methyl-D-aspartate (NMDA) receptors. Furthermore, our results show that these channels have a profound influence on the cell's response to sensory input.

METHODS

Animals and surgery

The weakly electric fish *Apteronotus leptorhynchus* was used exclusively in these experiments. Animals were housed in groups of three to six in 150-l tanks, temperature was maintained between 26 and 28°C, water conductivity varied from 400 to 800 μS, and pH was maintained between 6.8 and 7.2. The experiments were performed in Plexiglas tanks (30 × 30 × 10 cm) filled with water from the fish's home tank.

Surgical techniques were the same as described previously (Bastian 1996a,b). Briefly, animals were immobilized by intramuscular injection of 0.1–0.5 mg of Tubocurarine (Sigma, St. Louis, MO) and respirated via a mouth tube with aerated tank water at a flow rate of 10 ml/min. The fish was submerged in water except for the top of the head. To expose brain for recording, we first locally anesthetized the skin on the skull by applying 2% lidocaine and removed a thin strip of skin. A metal post was glued to the exposed area of the skull for stabilization. An access to the area of the cerebellum overlying the ELL was

achieved by drilling a hole of ~2 mm^2. The surface of the brain was kept covered by saline throughout the experiment. All animal procedures were approved by McGill University's Animal Care Committee.

Recordings

Intracellular recording techniques were the same as used previously (Bastian et al. 2002). Intracellular recordings were made with potassium chloride (3 M)– or potassium acetate (2 M)–filled 35- to 100-MΩ micropipettes and, confirming previous results (Bastian 1993), no differences were seen with either solution. Intracellular recording techniques with the pipette tip filled with 100 mM 1,2-bis(2-aminophenoxy)ethane-*N,N,N′,N′*-tetraacetic acid (BAPTA) were the same as used previously (Bastian 1998; Krahe et al. 2008). As in previous studies, it can take ≤10 min for BAPTA to diffuse into the cell and observe an effect depending on the resistance of the pipette. As such, it is possible to compare the activity of the same cell before and after BAPTA treatment in some cases. For these cells, control activity was taken during the first 1.5 min after impalement. We also recorded from pyramidal cells with and without BAPTA: for these experiments, BAPTA was allowed to diffuse for 5–10 min before the experiment was started. We recorded exclusively from the centrolateral and lateral segments because BAPTA was previously shown to have no effect in the centromedial segment (Krahe et al. 2008). Note that in vitro studies have shown that pyramidal cells in the centrolateral segment can show burst firing (Mehaffey et al. 2008a).

Extracellular single-unit recordings from pyramidal cells were made with metal-filled micropipettes (Frank and Becker 1964). Recording sites was determined from surface landmarks and recording depths were limited to centrolateral ELL segment. Both extracellularly and intracellularly recorded spikes were detected with CED 1401-plus hardware and SpikeII software, at resolution of 0.1 ms (Cambridge Electronic Design, Cambridge, UK). E-type pyramidal cells respond with increases in firing rate, whereas I-type pyramidal cells respond with decreases in firing rate to increases in EOD amplitude (Saunders and Bastian 1984). E- and I-type pyramidal cells were determined based on responses to sensory stimuli as done previously (Bastian et al. 2002).

Pharmacology

Previously established micropressure ejection techniques were used to locally apply glutamate (1 mM), UCL–1684 (UCL, 1 mM), APV (1 mM), and magnesium acetate (200 mM) within the ELL molecular layer containing the apical dendritic trees of a given cell (Bastian 1993; Bastian and Nguyenkim 2001; Chacron 2006; Chacron and Bastian 2008; Chacron et al. 2005c; Ellis et al. 2007a; Krahe et al. 2008; Mehaffey et al. 2008a). The agents were dissolved in saline. Multibarrel pipettes were pulled to a fine tip and subsequently broken to a total tip diameter of 10 μm. One barrel was filled with glutamate, whereas the remaining barrels were filled with the other solution. Once a recording from a pyramidal cell was established, the multibarrel pipette was slowly advanced into an appropriate region of the ELL molecular layer while periodically ejecting glutamate with pressure pulses of air (duration = 100 ms, pressure = 40 psi) using a picospritzer. The proximity of apical dendrite of a recorded cell was determined by a short-latency excitation of that cell (Bastian 1993). After satisfactory placement, each drug was delivered by a series

of pressure pulses (duration = 100 ms, pressure = 40 psi). We note that it can be difficult to find the right placement to actually have the two-barrel pipette within or near the apical dendritic tree. Extracellular recording are much less prone to be disturbed by manipulations than intracellular recordings. Therefore we switched to extracellular recordings when we performed the pharmacological manipulations as before (Chacron 2006). Drugs were purchased from Sigma and Tocris (Ellisville, MO). Previous studies have shown that drugs injected in this manner will not diffuse past the tractus stratum fibrosum and thereby will remain within the molecular layers of the ELL (Bastian 1993). However, such a technique will very often not affect a given pyramidal cell's entire dendritic tree, and the area of effect is drug dependent: larger molecules (e.g., APV and UCL) will have a smaller diffusion coefficient and will not diffuse as far from the ejection site on average as small ions (e.g., Mg^{2+}) (Bastian 1993).

Stimulation

Because the electric organ of *Apteronotus* is neurogenic, the EOD discharge persists after immobilization with curare-like drugs. All stimuli therefore consisted of modulations of the fish's own EOD by electric signals applied either globally via chloridized silver wire electrodes positioned 15 cm away from the fish on either side of the animal or locally via a small local dipole electrode positioned 1–3 mm from the skin (Bastian et al. 2002). The fish's EOD was recorded with chloridized silver wire electrodes positioned at the head and at the tail. The zero crossings of the amplified EOD signal (DAM50, World Precision Instruments, Sarasota, FL; band-pass filter between 300 Hz and 3 kHz) were detected by a window discriminator, which triggered a function generator to output a single-cycle sinusoid of slightly higher frequency than the fish's EOD. This created a train of single-cycle sinusoids that were phase-locked to the EOD. The train was then multiplied (MT3 multiplier, Tucker Davis Technologies, Gainesville, FL) with a modulation waveform produced by a computer. The resulting signal was attenuated (LAT45 attenuator, Leader Electronics, Cypress, CA) and fed into the tank via a stimulus isolator (A395 linear stimulus isolator, World Precision Instruments). Depending on the polarity of the signal relative to the fish's EOD, the signal led to an increase or a decrease in amplitude of the EOD.

Spontaneous neuronal activity was characterized by no external stimulus provided and the electrosensory system being driven only by the fish's unmodulated EOD. To determine response to stimuli, we used random AMs (RAMs). The modulation waveform for the RAMs was a low-pass-filtered (8th-order Butterworth filter, cut-off frequency: 120 Hz), zero-mean, Gaussian noise that lasted for 100 s. The amplitude of the global stimulus was calibrated at the position usually occupied by the fish but measured without the fish being in place. The reference amplitude at 0 dB was set to 1 mV/cm. Typical attenuation levels for global stimulation were −30 to −35 dB and for local stimulation were −25 to −30 dB. This setting for the local stimulus relative to the global stimulus was shown to provide equivalent drive to primary electrosensory afferents (Bastian et al. 2002; Chacron et al. 2005c). The modulation waveforms were sampled at 2 kHz.

Membrane time constants and input resistances were calculated from intracellular recordings by injecting a −0.12-nA current pulse lasting 1 s via the recording electrode ≥20 times and

averaging the membrane potential waveforms. The input resistance was calculated from Ohm's law as $R_{in} = \Delta V/\Delta I$, where ΔV is the change in membrane voltage caused by the change in current injection from 0 to −0.12 nA (Berman and Maler 1998b; Ellis et al. 2007a). The membrane time constant was measured by fitting an exponential function to the average membrane potential time course after the onset of the current pulse.

Data analysis

We segregated the spike train into bursts and isolated spikes using an interspike interval (ISI) threshold of 10 ms as done previously (Ellis et al. 2007a; Mehaffey et al. 2008b; Oswald et al. 2004): spikes belonging to ISIs that were less than this threshold were deemed part of a burst.

Responses to RAMs were accumulated as sequences of spike times for each cell and were converted to binary sequences sampled at 2 kHz as done previously (Chacron and Bastian 2008; Ellis et al. 2007a; Mehaffey et al. 2008a). The data analysis and stimulation protocols were similar to those used previously (Chacron 2006; Chacron et al. 2001a, 2003b, 2005a,b,c, 2007; Sadeghi et al. 2007). The coherence $C(f)$ between the binary sequence and the stimulus was calculated according to $C(f) = |P_{SX}(f)|^2/[P_{SS}(f)P_{XX}(f)]$, where P_{ss} and P_{xx} are the power spectra of the stimulus and the binary sequence, respectively, and P_{sx} is the cross-spectrum between the stimulus and the binary sequence. A lower bound on the rate density of information transmission at frequency f can was computed as $I_{lower}(f) = -\log_2[1 - C(f)]$ (Borst and Theunissen 1999). The mutual information rate MI_{lower} is obtained by integrating $I_{lower}(f)$ between 0 and the stimulus cut-off frequency. The mutual information rate measures the rate of information transmission per unit time and is measured in bits per second. X bits of information means that the system can theoretically distinguish between 2^X stimuli (Borst and Theunissen 1999). Because the mutual information rate increases approximately linearly as a function of the neuron's firing rate (Borst and Haag 2001), one can normalize the mutual information rate by the neuron's mean firing rate during stimulation f_0 to remove this dependency and therefore better compare neurons with different firing rates. We implemented this normalization in this study, and all the mutual information rates are thus measured in bits per spike: this represents the average amount of information that is transmitted by each action potential in the spike train. Statistical analysis was performed using the Matlab Statistics Toolbox.

We computed the spike-triggered average by averaging the stimulus waveform in a time window of 200 ms centered on each action potential as before (Chacron 2006). This measure gives the average stimulus waveform preceeding and following an action potential and is a useful way of characterizing a neuron's response to a time varying stimulus (Dayan and Abbott 2001).

We measured the amplitude of spike afterhyperpolarization in intracellular recordings by subtracting the average membrane potential in the 2 ms after an isolated action potential from the average membrane potential preceding that same action potential. An action potential was deemed to be isolated if there were no other spikes within a window of 200 ms centered on the action potential in question. To measure bursts depolarization, the spikes were truncated and the average voltage 100 ms before the burst was subtracted from the

average voltage during the burst. The decay time constant of the ISI probability density was measured by fitting an exponential function to the ISI probability density after the peak. This measure characterizes the tail of the ISI distribution and reflects changes in the ISI probability density that occur during burst firing: burst firing will typically increase the propensity of short ISIs and there will therefore be (relatively speaking) a lower proportion of long ISIs, thereby leading to a faster decay of the ISI probability density.

Quantities are reported as mean ± SE throughout this study. Analysis of statistical significance for same-cell intracellular and extracellular recordings was done using Wilcoxon signed-rank tests, and comparisons between different cells were done using Wilcoxon ranksum tests.

Modeling

We used previously described models of an ELL pyramidal cell. The first model is multicompartmental in nature and possesses a realistic dendritic geometry: it was previously described in detail (Doiron et al. 2001a,b). We used the same parameters as Doiron et al. (2001b) except that 500 excitatory synapses were scattered on the apical dendritic tree as done previously (Doiron et al. 2001a) and that a constant depolarizing current of 0.32 nA was injected in the somatic compartment to make the burst duration similar to that of the two-compartmental model described below (Doiron et al. 2002). The presynaptic spike trains consisted of independent and identically distributed Poisson processes each with firing rate 30 Hz. The conductance of each synapse after a presynaptic action potential at *time 0* is given by

$$g(t)=g_{\max}\frac{t}{\tau_{\text{syn}}}e^{1-\frac{t}{\tau_{\text{syn}}}}$$

where V is the postsynaptic membrane potential, $g_{\max} = 6 \times 10^{-5}$ μS, and $\tau_{\text{syn}} = 10$ ms. Each synapse is linked to Ca^{2+} dynamics that are described by the following equation

$$\frac{d[Ca]}{dt}=f_{\text{Ca}}(\alpha I_{\text{Ca}}-k_{\text{ex}}[Ca])$$

where [Ca] is the intracellular calcium concentration (in μM), f_{Ca} is a constant reflecting fraction of bounded to free Ca^{2+} (Wagner and Keizer 1994), $f_{\text{Ca}} = 0.03$/ms for control and $f_{\text{Ca}} = 0.0008$/ms for BAPTA, where the Ca^{2+} conversion constant is $\alpha = 0.0055$ μM/nA, and the Ca extrusion ratio is $k_{\text{ex}} = 1/\mu$M, and $I_{\text{Ca}} = -g(t)(V - V_{\text{Ca}})$. These values were determined from the data available (Mayer and Westbrook 1987; Nowak et al. 1984; Reynolds and Miller 1990). Anatomical studies have shown that NMDA receptors (Berman et al. 2001) are located in dendritic spines and that SK1 channels are also localized in the dendrites (Ellis et al. 2008). We assume that both are co-localized within spines and neglect calcium diffusion between spines. Thus the SK1 channel associated with each synapse was modeled by

$$I_{SK}=g_{SK}\frac{[Ca]}{[Ca]+k_{ca}}(V_K-V)$$

We used g_{SK} = 5.15 μS, V_{Ca} = 70 mV, k_{ca} = 0.4 μM, and V_K = −88.5 mV (Mayer and Westbrook 1987; Nowak et al. 1984; Reynolds and Miller 1990). Simulations of this model were performed using the NEURON simulation software (Hines and Carnevale 1997) with an integration time step of 0.025 ms. We note that the dendritic spike shape depends on the proximity of the recording site to the soma. We recorded from the proximal apical dendrite to match the spike shape obtained from experimental recordings and from our two-compartmental model described below.

Our second model consists of a two-compartmental reduction of the first one but contains all the essential elements to reproduce bursting seen experimentally in vitro (Doiron et al. 2002). This model consists of somatic and dendritic compartments connected through an axial resistance of $1/g_c$ (g_c: coupling conductance). Both compartments contain the essential spiking currents: fast inward Na^+ ($I_{Na,s}$, $I_{Na,d}$) and outward delayed rectifying (Dr) K^+ ($I_{Dr,s}$, $I_{Dr,d}$), and passive leak currents (I_{leak}). The presence of spiking currents in the dendrite enables the active backpropagation of somatic action potentials required for bursting. The membrane potentials at the soma, V_s, and the dendrite, V_d, are determined using a Hodgkin–Huxley–like formalism. The original model (Doiron et al. 2002) comprised six nonlinear differential equations. To simulate in vivo conditions, we expanded this model by incorporating the intracellular Ca^{2+} dynamics into the dendritic compartment. The NMDA current (I_{Ca}) provides Ca^{2+} influx (Ascher and Nowak 1988; MacDermott et al. 1986), which activates the dendritic SK current (I_{SK}) (Bond et al. 1999; Faber et al. 2005; Ngo-Anh et al. 2005; Vergara et al. 1998).

The voltage at the soma (V_S) and dendrite (V_D) is described by the following equation

$$C_m\frac{dV_S}{dt}=I_{app}+I_{NaS}+I_{DrS}+\frac{g_c}{k}(V_D-V_S)+g_L(V_L-V_S)$$
$$C_m\frac{dV_D}{dt}=I_{NaD}+I_{DrD}+\frac{g_c}{1-k}(V_S-V_D)+g_L(V_L-V_D)+I_{Ca}+I_{SK}$$

where the currents are given by

$$\begin{aligned}
I_{NaS} &= g_{NaS}m_{\infty,S}^2(1-n_S)(V_{Na}-V_S)\\
I_{DrS} &= g_{DrS}n_S^2(V_K-V_S)\\
I_{NaD} &= g_{NaD}m_D^2h_D(V_{Na}-V_D)\\
I_{DrD} &= g_{DrD}n_D^2p_D(V_K-V_D)\\
I_{Ca} &= g_{NMDA}s(V_{Ca}-V_D)\\
I_{SK} &= g_{SK}\frac{[Ca]}{[Ca]+k_{ca}}(V_K-V_D)
\end{aligned}$$

The parameter g is a maximal conductance (g_{max}, mS/cm^2), whereas m and s are activation variables, and h, n, and p are inactivation variables. Each is described by the following equation

$$\frac{dx}{dt}=\frac{x_\infty(V)-x}{\tau_x}$$

where $x_\infty(V)$ is the infinite conductance curve and τ_x is the time constant. The infinite conductance curve is modeled as a sigmoid

$$x_\infty(V)=\frac{1}{1+\exp\left(\frac{V_x-V}{S_x}\right)}$$

and the values for τ_x, V_x, s_x, and g_{max} for each current are as follows: τ_{nS} = 0.39 ms, τ_{hD} = 1 ms, τ_{nD} = 0.9 ms, τ_{pD} = 5 ms, τ_s = 5 ms, s_{mS} = 3, s_{nS} =3, s_{md} = 5, s_{hD} = −5, s_{nD} = 5, s_{pD} = −6, s_s = 6, V_{mS} = −40 mV, V_{nS} = − 40 mV, V_{mD} = − 40 mV, V_{hD} = − 52 mV, V_{nD} = − 40 mV, V_{pD} = − 65 mV, V_s =50 mV, g_{NaS} =55 mS/cm^2, g_{DrS} = 20 mS/cm^2, g_{NaD} =5 mS/cm^2, g_{DrD} =15 mS/cm^2, g_{SK} =7 mS/cm^2, and g_{NMDA}= 20 mS/cm^2. To mimic blockade of SK channels by UCL, we set g_{SK} = 3 mS/cm^2 because it is very likely that UCL does not block all dendritic SK channels in ELL pyramidal cells as mentioned above. We fitted our model to available data (Mayer and Westbrook 1987; Nowak et al. 1984; Reynolds and Miller 1990). The Ca^{2+} dynamics are described by the same equation as for the other model

$$\frac{d[Ca]}{dt}=f_{Ca}(\alpha I_{Ca}-k_{ex}[Ca])$$

where f_{Ca} = 0.003/ms for control and f_{Ca} = 0.008/ms for BAPTA; α = 0.0055 μM/nA, k_{ex} = 1/μM, and k_{ca} = 0.4 μM.

Other parameter values are as follows: ratio of somatic to total area, k = 0.4; the reversal potentials, V_{Na} = 40 mV, V_K = − 88.5 mV, V_{Ca} = 70 mV, V_{leak} = −70 mV; membrane capacitance, C_m = 1μF/cm^2; g_{leak} = 0.18 mS/cm^2 and g_c = 1 mS/cm^2; applied current, I_{app} = 12 nA. The model equations were integrated using an forward Euler algorithm with a time step of 0.02 ms.

RESULTS

Differences between in vitro and in vivo bursting

Figure 1 summarizes the intrinsic bursting properties of pyramidal cells obtained in vitro (Lemon and Turner 2000). Somatic action potentials backpropagate into the proximal apical dendrites where they trigger a wider dendritic spike that propagates back to the soma, leading to a DAP (Fig. 1*A*). Both somatic (Fig. 1*B*) and dendritic (Fig. 1*C*) recordings obtained in vitro show characteristic features of intrinsic burst firing in ELL pyramidal cells. The DAP at the soma grows in size throughout the burst (Fig. 1*B*, arrows), which leads to a progressive depolarization and a shortening of the ISI throughout the burst (Fig. 1*B*). The burst terminates with a characteristic doublet when the ISI becomes shorter than the dendritic refractory period (Fig. 1*B*, asterisk) (Noonan et al. 2003), leading to dendritic

failure characterized by the absence of a dendritic spike (Fig. 1*C*, asterisk). The lack of a DAP causes a bAHP in the soma (Fig. 1*B*).

We recorded intracellularly from $n = 31$ ELL pyramidal cells in vivo under baseline conditions (i.e., no EOD modulations). We pooled recordings from E- and I-type pyramidal cells because no significant differences were seen. Although pyramidal cells tended to fire clusters of action potentials in vivo, somatic action potentials were followed by pronounced AHPs (Fig. 1*D*), with no evidence for DAPs or bAHPs. Dendritic spikes were not followed by as prominent of an AHP (Fig. 1*E*) but no dendritic failures were observed because spike height remained constant throughout repetitive firing. These results show that in vivo conditions can have a major impact on burst firing seen in vitro.

Previous studies have found large heterogeneities amonst pyramidal cells: cells whose somata are found most superficially within the pyramidal cell layer have the most extensive apical dendritic trees, whereas cells whose somata are found deep within the pyramidal cell layer have the smallest apical dendritic trees and have large firing rates (Bastian and Nguyenkim 2001; Bastian et al. 2004). In particular, a strong negative correlation ($R = -0.81$) between apical dendritic length and baseline firing rate has been previously established by several studies, enabling us to gain information to a cell's morphology from measurements of the baseline firing rate (Bastian and Nguyenkim 2001; Bastian et al. 2004). Furthermore, previous studies have suggested that cells whose baseline firing rates are <10 Hz correspond to superficial pyramidal cells, whereas cells whose baseline firing rates are >30 Hz correspond to deep pyramidal cells (Bastian et al. 2004; Chacron 2006; Chacron et al. 2005c). It is therefore possible that our recordings performed in vivo were from different pyramidal cell than in vitro recordings that are mostly from superficial pyramidal cells (Ellis et al. 2007b). We thus explored the relationship between firing rate and spiking properties such as spike width and refractory period (note that we defined the refractory period as the minimum value of the ISI, which is not necessarily equal to the absolute refractory period as shown below): we found that both quantities were strongly negatively correlated with firing rate (Fig. 2, *A* and *B*; action potential width: $R = -0.6214$, $P = 0.0078$, $n = 17$; refractory period: $R = -0.8158$, $P \ll 10^{-3}$, $n = 17$). Although our values for spike width were quite similar to those from in vitro recordings (Berman and Maler 1998b; Mehaffey et al. 2008b), our values for the refractory period were high. Indeed, cells with the lowest firing rates that correspond to superficial pyramidal cells with the largest dendritic trees (Bastian and Nguyenkim 2001) had a mean refractory period of 8.56 ± 0.6743 ms ($n = 5$), which is larger than the range of ISIs that lead to dendritic failure in vitro (Doiron et al. 2003b; Noonan et al. 2003). In no case did we observe either dendritic failure or bAHPs in our in vivo recordings of baseline activity. As such, these results suggest that, although the overall spike shape is similar in both in vivo and in vitro recordings, superficial pyramidal cells have a tendency to not fire action potentials in vivo within the time interval that leads to dendritic failure in vitro.

BAPTA induces in vitro–like burst firing in vivo

What could cause the large refractory periods observed in vivo in ELL pyramidal cells? We hypothesized that the AHPs after each action potential that are usually mediated by calcium-

activated potassium channels (Sah 1996) might be responsible. We therefore applied the calcium chelator BAPTA that has been shown previously to reduce the AHP in vivo (Krahe et al. 2008). Diffusion of BAPTA inside the cell had a significant effect on pyramidal cell activity in vivo: it eliminated the AHP after somatic action potentials (Fig. 3*A*) and caused the appearance of characteristic burst doublets and bAHPs. BAPTA also affected dendritic recordings, showing an underlying depolarization throughout the burst that was terminated by dendritic failure (Fig. 3*B*). BAPTA therefore induced burst firing in vivo that has the same prominent characteristics as burst firing seen in vitro. Changes in the cell's firing properties were reflected in the ISI distribution (Fig. 3*C*): treatment with BAPTA significantly increased the proportion of short ISIs around 3–5 ms. We further quantified the structure in the spike train by computing the ISI return map (i.e., a plot of each ISI as a function of the preceeding one): a representative example shows that the ISI return map displays a structure characteristic of a bursting ELL pyramidal cell in vitro (Ellis et al. 2007b) (Fig. 3*D*).

We further quantified the effects of BAPTA by computing several quantities of interest: the burst fraction, the mean firing rate, the refractory period, the magnitude of the AHP, the average number of spikes per burst, the decay time constant of the ISI distribution, and the average membrane potential depolarization. We found that BAPTA treatment leads to significant changes in all these quantities: BAPTA significantly decreased the refractory period (Fig. 4*A*; control, 8.40 ± 0.63 ms; BAPTA, 3.31 ± 0.31 ms; $n = 24$; percent change in mean: 61%; $P \ll 10^{-3}$, Wilcoxon rank sum test) and increased the burst fraction (Fig. 4*B*; control, 0.13 ± 0.035; BAPTA, 0.74 ± 0.04, $n = 26$; percent change in mean: 469%; $P \ll 10^{-3}$, Wilcoxon rank sum test). As a consequence of the increased burst fraction, the ISI distribution shifted toward smaller values, and the time constant of the distribution significantly decreased contingent on BAPTA treatment (Fig. 4*C*). The average number of spikes per burst increased by 600% (Fig. 4*D*). BAPTA significantly decreased the AHP magnitude (Fig. 4*E*), confirming previous results (Krahe et al. 2008). BAPTA also significantly increased the membrane potential depolarization during a burst (Fig. 4*F*).

BAPTA also affected the passive properties of ELL pyramidal cells: the membrane time constant was significantly increased (control, 5.79 ± 1.14 ms; BAPTA, 13.69 ± 2.93 ms; $n = 7$; percent change in mean: 136%; $P = 0.0156$, Wilcoxon sign-rank test) and the input resistance was significantly increased (control, 8.33 ± 1.38 MΩ; BAPTA, 16.56 ± 3.14 MΩ; $n = 7$; percent change in mean: 99%; $P = 0.0156$, Wilcoxon sign-rank test). BAPTA also caused a slight but significant hyperpolarization in the resting membrane potential (control, −67.96 ± 0.77 mV; BAPTA, −71.38 ± 1.40 mV; $n = 9$; percent change in mean: 5%; $P = 0.0039$, Wilcoxon sign-rank test).

We next looked at whether BAPTA affected deep versus superficial pyramidal cells differentially. We plotted the increase in burst fraction induced by BAPTA as a function of the cell's baseline firing under control conditions (Fig. 4*G*) and found a significant negative correlation between both quantities ($R = -0.78$, $P \ll 10^{-3}$, $n = 24$), indicating that BAPTA had a strong effect on pyramidal cells with low firing rates and very little effect on pyramidal cells with higher firing rates. Because previous studies have found a strong correlation between pyramidal cell dendritic morphology and the baseline firing rate (Bastian and

Nguyenkim 2001), these results imply that BAPTA primarily affects cells with extensive dendritic trees.

BAPTA treatment decreases information transmission by pyramidal cells

We also looked at the consequences of BAPTA treatment on information transmission by pyramidal cells using both local and global stimulation geometries that respectively mimic prey and communication stimuli. BAPTA significantly reduced the magnitude of the spike-triggered average for both global (Fig. 4*A*) and local (Fig. 4*C*) stimulation geometries. This reduced response leads to a significant decrease in the mutual information rate *MI* obtained for both global (Fig. 4*B*; control, 5.16 ± 1.81 bits/spike; BAPTA, 0.77 ± 0.25 bits/spike; $n = 12$; percent change in mean: 85%; $P = 0.0319$, Wilcoxon rank sum test) and local (Fig. 4*D*) stimulation (control, 1.75 ± 0.62 bits/spike; BAPTA, 0.39 ± 0.14 bits/spike; $n = 11$; percent change in mean: 78%; $P = 0.0459$, Wilcoxon rank sum test). We further studied this effect by looking how the addition of a stimulus affected the structure of the spike train as quantified by the ISI return map. Under control conditions, there are significant differences between the ISI return map for baseline and stimulated activity, indicating that the stimulus has an effect on the spike train (Fig. 5*E*). However, the ISI return maps obtained under baseline and stimulated conditions for BAPTA showed large degrees of overlap particularly for ISIs <10 ms (i.e., the ISIs that we took to belong to bursts; Fig. 5*F*), indicating that the cell's strong bursting dynamics under baseline conditions were not modulated strongly by the addition of a sensory stimulus.

SK current affect pyramidal cell activity in vivo

We turned our attention to the mechanisms that are affected by BAPTA in vivo. Small conductance calcium-activated potassium (SK) channels open in response to elevations in the intracellular calcium concentration and produce an AHP after each action potential (Faber and Sah 2007; Kohler et al. 1996). Both in situ hybridization and immunohistochemical labeling studies have shown that only the SK1 and SK2 subtypes are expressed in the ELL, with SK1 localized at the apical dendrites of both E- and I-type pyramidal neurons, and SK2 channels localized at the soma of E-type pyramidal neurons only (Ellis et al. 2007b, 2008). These studies further showed differential expression of SK channels based on pyramidal cell class: SK channels of both subtypes were strongly expressed in superficial pyramidal cells and very weakly expressed in deep pyramidal cells. Although some of the effects seen here could also be because of BAPTA affecting big conductance calcium-activated potassium (BK) channels, application of the selective BK antagonist iberiotoxin did not affect ELL pyramidal cell firing properties (Krahe et al. 2008). We therefore focused on SK channels.

Because we found that BAPTA had an effect on both E- and I-type pyramidal cells in vivo, we hypothesized that the effects of BAPTA were primarily caused by reducing the effect of dendritic SK1 channels instead of somatic SK2 channels. Because previous studies have shown that the SK channel antagonist apamin had no effect in vivo when applied to the ELL molecular layers (Krahe et al. 2008), we instead used the potent SK channel blocker UCL-1684 (UCL) during extracellular recordings of pyramidal cell activity. Application of UCL significantly increased firing rate (control, 8.93 ± 1.48 Hz; UCL, 10.94 ± 1.78 Hz; $n =$

11; percent change in mean: 22%; $P = 0.018$, Wilcoxon sign-rank test) and had drastic effects on pyramidal cell activity by inducing burst firing similar to that seen with BAPTA (Fig. 6, *A* and *B*), the ISI distribution shifted toward smaller values, and the peak of the distribution became more pronounced (Fig. 6*C*). The burst fraction was significantly increased (Fig. 6*D*; control, 0.085 ± 0.03; UCL, 0.21 ± 0.057, $n = 11$; percent change in mean: −147%; $P = 0.0294$), the cell's refractory period decreased significantly (Fig. 6*E*; control, 8.8 ± 1.0 ms; UCL, 7.4 ± 0.9 ms; $n = 11$; percent change in mean: 16%; $P = 0.0044$, Wilcoxon sign-rank test), and the time constant of the ISI distribution decreased significantly (Fig. 6*F*; control, 28.1 ± 1.0 ms; UCL, 10.3 ± 1.8 ms; $n = 11$; percent change in mean: 64%; $P = 0.00976$, Wilcoxon sign-rank test).

Application of UCL also affected information transmission by pyramidal cells by significantly reducing the magnitude of the spike-triggered average for global stimulation (Fig. 6*G*; control, 1.0 ± 0.12; UCL, 0.74 ± 0.12; $n = 13$; percent change in mean: 25%; $P = 0.01$, Wilcoxon sign-rank test). This leads to a significant decrease in the mutual information rate *MI* (Fig. 6*H*; control, 0.59 ± 0.14 bits/spike; UCL, 0.38 ± 0.12 bits/ spike; $n = 13$; percent change in mean: 34%; $P = 0.04$, Wilcoxon sign-rank test).

Contribution of NMDA receptors toward Ca^{2+} entry into the membrane

Given that the primary effect of BAPTA is to bind to Ca^{2+} ions, the dramatic change in bursting might be attributed to the intracellular Ca^{2+} dynamics. Because changes in bursting were also seen after the injection of an SK channel blocker in the apical dendrites, the source of calcium was probably located within the dendrites. Because previous studies have shown that NMDA channels are abundant in the dendrites of the ELL pyramidal cells (Berman et al. 2001; Bottai et al. 1997; Dunn et al. 1999; Harvey-Girard and Dunn 2003), we hypothesized that NMDA channels provided at least part of the intracellular Ca^{2+} necessary for SK1 channel activation (Faber et al. 2005; Garaschuk et al. 1996; Glitsch 2008; Koh et al. 1995; Ngo-Anh et al. 2005).

To test this hypothesis, we ejected Mg^{2+} within the ELL molecular layers. Mg^{2+} also had drastic effects on pyramidal cell activity in vivo, inducing burst firing (Fig. 7, *A* and *B*). Like BAPTA and UCL, injection of Mg^{2+} increased the mean firing rate (control, 13.97 ± 1.36 Hz; Mg^{2+}, 16.7 ± 1.42 Hz; $n = 13$; percent change in mean: 19%; $P = 0.006$, Wilcoxon sign-rank test); it also shifted the ISI distribution shifted toward smaller values (Fig. 7*C*), the burst fraction increased (Fig. 7*D*; control, 0.29 ± 0.047; Mg^{2+}, 0.5 ± 0.05, $n = 13$; percent change in mean: −72%; $P = 0.0089$, Wilcoxon sign-rank test), the cell's refractory period decreased (Fig. 7*E*; control, 6.5 ± 0.5 ms; Mg^{2+}, 4.9 ± 0.2 ms; $n = 13$; percent change in mean: 25%; $P = 0.0263$, Wilcoxon sign-ranked test), and the time constant of the ISI distribution decreased significantly (Fig. 7*F*; control, 10.2 ± 0.2 ms; Mg^{2+}, 5.7 ± 1.0 ms; $n = 13$; percent change in mean: 43%; $P = 0.0258$, Wilcoxon sign-rank test).

The effects of UCL and Mg^{2+} were smaller in magnitude than the effects of BAPTA, and this could be because of the fact that the ejection only affected part of the large apical dendritic tree of ELL pyramidal cells as previously observed (Bastian 1993). We also ejected the selective NMDA antagonist APV, which had a qualitatively similar effect to that of magnesium but much weaker ($n = 3$, data not shown). This is perhaps because APV, being a

large molecule, will not diffuse as far as the smaller Mg^{2+} ion and thus will not block as large a portion of the cell's apical dendritic tree. Nevertheless, these results strongly suggest that NMDA current provide intracellular Ca^{2+} in vivo, which activate dendritic SK1 channels, giving rise to an AHP that counteracts the DAP under baseline conditions in vivo.

Modeling the effects of dendritic SK channels on burst firing

To study how disruption of intracellular Ca^{2+} by BAPTA reduces information transmission by pyramidal cells, we used two mathematical models of an ELL pyramidal cell. The first model is multicompartmental and possesses a realistic dendritic geometry (Doiron et al. 2001b). The second consists of a two-dimensional reduction of the first one in which the dendritic tree is "collapsed" to a single compartment. This minimal model has been shown to reproduce the intrinsic pyramidal cell burst firing observed in vitro (Doiron et al. 2002). We added both synaptic input and SK currents to the dendritic compartments of both models, with the synaptic current providing a source of Ca^{2+} to the dendrite, thereby activating dendritic SK channels as detailed in METHODS.

With the synaptic conductance $g_{max} = 0$, the large compartmental model produced bursting similar to that seen in vitro that terminated with dendritic failures (Doiron et al. 2001b, 2002) (Fig. 8*A*). Adding the synaptic input ($g_{max} = 6 \times 10^{-5}$ μS) has drastic effects on bursting dynamics: the dendritic failures and associated changes in spike height disappeared producing a strong resemblance to in vivo bursting (Fig. 8*B*). We attempted to reproduce the effects of BAPTA in our model: because Ca^{2+} absorption by BAPTA slows down accumulation of intracellular free Ca^{2+}, we modeled the effect of BAPTA as a decrease in fraction of free Ca^{2+} (f_{Ca}). We found that decreasing f_{Ca} induced bursts riding on depolarizations that were terminated with dendritic failures (Fig. 8*C*), similarly to what has been observed experimentally.

To better understand these results, we added NMDA and SK currents to the reduced two-compartmental model. Without the NMDA current ($g_{nmda} = 0$), the model produces bursting similar to that seen in the large compartmental model (cf. Fig. 8, *D* and *A*). Addition of the NMDA current ($g_{nmda} = 20$ mS/cm^2) had similar effects to those seen in the large compartmental model (cf. Fig. 8, *E* and *B*). Decreasing the fraction of free Ca^{2+} (f_{Ca}) had a similar effect to that seen in the large compartmental model in that it produced bursts that were terminated by a dendritic failure (cf. Fig. 8, *F* and *C*). Further study in our model showed the mechanism by which SK channels lead to early termination of the burst. We plotted the intracellular calcium concentration [Ca] and the SK current I_{SK} under all three conditions. Of course, setting $g_{nmda} = 0$ causes no calcium accumulation during spiking (Fig. 8*G*). Setting $g_{nmda} = 20$ mS/cm^2 and $f_{Ca} = 0.003$/ms causes rapid accumulation of calcium during repetitive spiking (Fig. 8*H*). Note that the cumulative increase in the SK current is not caused by the SK conductance because it saturates well before 10 μM with our parameter values. Instead, these are caused by the battery term ($V - V_k$) and the growing DAP throughout the burst (Lemon and Turner 2000). Finally, setting $g_{nmda} = 20$ mS/cm^2 and $f_{Ca} = 0.008$/ms causes a slower accumulation of calcium during repetitive spiking (Fig. 8*I*). These changes in the accumulation of intracellular calcium during spiking have important consequences for the SK current. Of course, we have $I_{SK} = 0$ when $g_{nmda} = 0$ (Fig. 8*J*).

However, setting g_{nmda} = 20 mS/cm^2 and f_{Ca} = 0.003/ms causes a rapid cumulative activation of the SK current during repetitive firing (Fig. 8*K*), which causes a growing AHP and leads to an early burst termination. During the silent phase, the Ca^{2+} concentration slowly decreases until the next period of spiking activity is initiated. Setting f_{Ca} = 0.008/ms slows down the accumulation of calcium during repetitive firing (Fig. 8*I*), which slows down the cumulative activation of I_{SK} (Fig. 8*L*), which leads to a slower growth of the AHP. This slower growth is not sufficient to counteract the DAP growth during the burst and the burst thus terminates with a dendritic failure.

We quantified the changes in spiking activity in the reduced model under simulated control, BAPTA, and UCL (mimicking the effects of blocking SK channels) conditions using measures similar to those used in the experimental data. Overall, the model under simulated BAPTA and UCL conditions had a lower refractory period (Fig. 9*A*), a higher burst fraction (Fig. 9*B*), a shorter ISI histogram time constant (Fig. 9*C*), a larger number of spikes per burst (Fig. 9*D*), a smaller AHP size (Fig. 9*E*), and a larger burst depolarization (Fig. 9*F*).

Our models thus propose a mechanism by which BAPTA modulates burst firing in ELL pyramidal cells: BAPTA binds intracellular calcium and thus the intracellular calcium concentration does not increase as fast during repetitive firing, thereby preventing early termination of the burst by the AHP. Therefore the SK current does not increase enough during the burst to prevent DAP from coming back to the soma, and the burst terminates with a dendritic failure (Fig. 8, *C* and *F*).

Reduced model reproduces the decrease in information transmission seen experimentally with BAPTA and UCL

We added the same RAM stimuli as we used in experiments as a current injection to the somatic compartment of the reduced two-compartmental model to mimic the input from electroreceptor afferents as a result of global stimulation. Similar to the in vivo recordings data (Fig. 5), decreasing f_{Ca} in the model decreased both the spike-triggered average amplitude (Fig. 10*A*) and the mutual information rate *MI* (Fig. 10*B*) similarly to what has been observed experimentally. We also mimicked blockade of SK channels by UCL in the model and found results similar to those obtained under simulated BAPTA conditions (Fig. 10, *A* and *B*). These results confirm that it is the cell's intrinsic dynamics that interfere with information transmission.

DISCUSSION

We studied the characteristics of burst firing in ELL pyramidal cells in vivo and found significant differences with burst firing properties found in vitro. Specifically, we found that, in vivo, most cells showed refractory periods that were quite large (5–12 ms) and did not show burst doublets or dendritic failures that are characteristic of burst firing in vitro. We found that the calcium chelator BAPTA had a significant effect on firing activity: BAPTA induced burst firing in vivo that had similar characteristics to the burst firing seen in vitro and strongly interfered with the cell's ability to encode a time varying stimulus. BAPTA increased both the membrane time constant and input resistance of ELL pyramidal cells and also caused a slight hyperpolarization in the membrane potential. Further analysis showed

that it was because the bursting dynamics had a characteristic structure that was not modulated by the addition of the stimulus.

We also studied the causes for the differences between burst firing in vivo and in vitro. We found that UCL, an SK channel antagonist, and magnesium, an NMDA channel blocker, both induced firing patterns that were similar to that seen with BAPTA. Therefore we concluded that it was Ca^{2+} entering the cell via dendritic NMDA receptors that activated dendritic SK1 channels. Both a detailed multicompartmental model and a two-compartment model of burst firing in vitro incorporating both dendritic synaptic input and SK conductances could reproduce the effects of BAPTA on both burst firing and encoding of time varying stimuli. The similarities between the detailed compartmental and reduced models suggest that the precise details of the dendritic tree structure are not important for the effect. Our results are thus likely applicable to other neurons with a dendritic structure different from that of ELL pyramidal cells. Detailed analysis of the reduced model showed that accumulation of Ca^{2+} during repetitive firing would lead to early termination of the burst by cumulative activation of the SK current, which leads to AHP growth under control conditions and further supports the evidence that it is the cell's intrinsic dynamics that interfere with the cell's ability to encode a time-varying stimulus.

Our results showed that in vivo conditions can have a significant effect on intrinsic bursting dynamics that are observed in vitro. Previous reports have found that the high-conductance state of neurons in vivo can have a significant influence on the processing of synaptic input and intrinsic burst dynamics in thalamic relay neurons (Destexhe and Paré 1999; Wolfart et al. 2005). However, it was the synaptic noise that was responsible for the observed changes. Here, we found that activation of SK channels was responsible for the altered burst dynamics. Our results have shown that these burst dynamics made pyramidal cells less responsive to a time-varying sensory input. However, in vitro studies have shown that ELL pyramidal cells responded strongly to current injection mimicking sensory stimulation in vivo (Ellis et al. 2007a; Mehaffey et al. 2008a; Oswald et al. 2004). In fact, recent studies have shown that in vitro bursting could encode the low-frequency components of a time varying current input with the doublet interval coding for stimulus intensity and slope (Doiron et al. 2007; Oswald et al. 2007). Our results showed that these mechanisms do not seem to be present in vivo because there was no significant correlation between the input and the cell's spike train after BAPTA treatment. A potential explanation for this discrepancy is that the voltage deflections caused by synaptic current would be smaller in vivo because of the high conductance state of the neuron and would thus have a smaller influence on the firing pattern overall. Moreover, synaptic input that is not correlated with the stimulus would act as noise, thereby reducing the response seen in vivo. Another explanation is that incoming sensory input arrives in the basilar dendrites of E-cells and inhibitory interneurons (Maler 1979), whereas all the experiments done in vitro rely on current injection in the soma (Oswald et al. 2004). Further studies expanding on this one are necessary to understand the differences between the firing properties of ELL pyramidal cells in vitro and in vivo.

We found that BAPTA had significant effects on the passive properties of ELL pyramidal cells in vivo. Both the input resistance and membrane time constants of ELL pyramidal cells

in vivo are ~50% of the values observed in vitro, respectively (Berman and Maler 1998b), which is consistent with the high-conductance state of neurons in vivo. BAPTA treatment increased both of these quantities, which is consistent with BAPTA effectively reducing the Ca^{2+} entering the cell via NMDA receptors and thereby reducing the activation of dendritic and somatic SK channels. BAPTA also caused a slight hyperpolarization in the resting membrane potential, which is also consistent with it reducing the Ca^{2+} current entering via NMDA receptors. BAPTA also caused the bursts to ride on top of large depolarizations, which we assume to be DAP mediated.

We showed a novel function for SK channels: namely the gating of information transmission through the early termination of an intrinsic bursting mechanism that is observed in vitro. SK channels are ubiquitous throughout the CNS and have been shown be implicated in regulating neural firing patterns such as burst termination (Swensen and Bean 2003) and adaptation to transient stimuli (Sah and Faber 2002), as reviewed recently (Bond et al. 2005). The distribution of SK channels in the ELL has been recently determined (Ellis et al. 2008). Moreover, a recent study has shown that somatic SK2 channels mediate adaptation and reduce the tuning of E-type ELL pyramidal cells to low frequencies (Ellis et al. 2007b) as predicted from theoretical studies (Benda and Herz 2003). Our results showed that dendritic SK1 channels play a large role in regulating ELL pyramidal cell burst dynamics and information processing in vivo because the effect of BAPTA was qualitatively similar in E- and I-cells.

An important question pertains to the actual source of calcium for dendritic SK1 channels. Although previous studies have found no evidence for voltage-gated calcium channels in ELL pyramidal cells, these same studies have found evidence for the presence of NMDA receptors (Berman and Maler 1998a,b,c). These electrophysiological studies are supported by immunohistochemistry studies showing that NMDA receptors are located within dendritic spines on the pyramidal cell dendrites (Berman et al. 2001). SK channels have recently been cloned for *Apteronotus leptorhynchus,* and it was found that only the SK1 and SK2 subunits are located within the ELL (Ellis et al. 2007b, 2008). Although SK2 channels are located exclusively on the somata of E-cells, SK1 channels are located on the apical dendrites of both E- and I-cells (Ellis et al. 2008). It is thus very likely that the source of calcium that activates SK1 channels comes from NMDA receptors as has been proposed before (Faber et al. 2005; Ngo-Anh et al. 2005). Our results using Mg^{2+} and APV strongly suggest that calcium entering via NMDA receptors activates SK1 channels in ELL pyramidal cells but do not preclude other mechanisms such as release of calcium from intracellular calcium stores involving Ryanodine and IP3 receptors (Berman et al. 1995; Zupanc et al. 1992). Further studies are necessary to determine the source of calcium activating the SK1 channels and are beyond the scope of this study.

We showed that burst firing in vivo under baseline conditions was quite different from under in vitro conditions. The following questions arise: is in vitro burst firing merely an artifact of the low-conductance and quiescent state of ELL pyramidal cells in vitro or can it serve a function in vivo? Our results suggest the latter because we were able to observe in vitro–like burst firing in vivo. In fact, because the absolute refractory period of deep pyramidal cells is less than that of superficial pyramidal cells, the former are thus more likely to show in vitro–

like bursting in vivo, and dendritic failures can sometimes be observed in pyramidal cells with high firing rates (>28 Hz) under sensory stimulation (Oswald et al. 2004). We hypothesize that in vitro–like bursts would be observed in superficial pyramidal cells under conditions in which the SK1 channels are downregulated. It is possible that this action could be caused by neuromodulators. The effects of neuromodulators in the ELL have just begun to be studied (Ellis et al. 2007a), and recent studies have suggested that acetylcholine might downregulate the AHP in ELL pyramidal cells (Mehaffey et al. 2008a). However, the behavioral conditions that activate cholinergic receptors in the ELL are currently unknown, and further studies are needed.

Another important question pertains to a putative function for in vitro–like burst firing. Our results showed that BAPTA almost abolished the response to local prey-like stimulation, strongly speaking against the hypothesis that in vitro–like bursts being used during prey detection in weakly electric fish as has been previously suggested (Oswald et al. 2004). This function is more likely to be performed by in vivo bursting because it was shown that this bursting was more present under prey-like stimulation than communication-like stimulation (Chacron and Bastian 2008). However, our results do not necessarily preclude that in vitro–like bursting could be used to detect other behaviorally relevant stimuli. Previous studies have shown that these bursts have the same all-or-none property as single action potentials, namely excitability (Laing et al. 2003): this property of in vitro bursting implies that its time course is largely independent of the stimulus once it has been initiated. This suggests that in vitro–like bursts may be better suited at detecting features in the animal's environment, preferably strong transient stimuli such as communication calls from conspecifics (Zakon et al. 2002), but further studies are needed to ascertain this fact. We note that previous studies have proposed and shown feature detection by bursts (Chacron et al. 2001b, 2004; Gabbiani et al. 1996; Kepecs and Lisman 2003; Kepecs et al. 2002; Lesica and Stanley 2004). However, our results suggest that some bursts would be used for feature detection, whereas other bursts may be used for stimulus estimation.

Finally, our results are consistent with a growing body of evidence for dendritic computation. It has been previously proposed that dendrites perform important computations such as filtering synaptic input or coincidence detection (Hausser and Mel 2003; London and Hausser 2005). Our results add to these in showing that dendrites have the ability to gate information transmission in sensory neurons in vivo. Gating of information transmission has been observed in the thalamus, where cortical feedback can modulate a relay neuron's intrinsic burst firing related to the animal's state of vigilance (Llinas and Steriade 2006; Sherman and Guillery 2002). However, bursts of action potentials have also been observed from in vivo recordings from thalamic relay neurons under awake conditions, where they encode the low-frequency components of visual input (Lesica and Stanley 2004). Previous studies have shown that SK channels can also oppose burst firing in nigral dopamine neurons, thereby regulating the time course of dopamine release (Gonon 1988; Johnson and Wu 2004; Ping and Shepard 1996). The omnipresence of intrinsic burst mechanisms, SK channels, and NMDA receptors throughout the CNS make it very likely that a mechanism similar to the one shown here is present in other systems and might explain the decreased burst firing observed in vivo in some systems (Steriade 2001).

Acknowledgments

GRANTS

This work was supported by the Canadian Institutes of Health Research, the Canada Foundation for Innovation, and a Canada Research Chair to M. J. Chacron.

References

Ascher P, Nowak L. The role of divalent cations in the N-methyl-D-aspartate responses of mouse central neurones in culture. J Physiol. 1988; 399:247–266. [PubMed: 2457089]

Bastian J. The role of amino acid neurotransmitters in the descending control of electroreception. J Comp Physiol [A]. 1993; 172:409–423.

Bastian J. Plasticity in an electrosensory system. I. General features of a dynamic sensory filter. J Neurophysiol. 1996a; 76:2483–2496. [PubMed: 8899621]

Bastian J. Plasticity in an electrosensory system. II. Postsynaptic events associated with a dynamic sensory filter. J Neurophysiol. 1996b; 76:2497–2507. [PubMed: 8899622]

Bastian J. Modulation of calcium-dependent postsynaptic depression contributes to an adaptive sensory filter. J Neurophysiol. 1998; 80:3352–3355. [PubMed: 9862931]

Bastian J, Chacron MJ, Maler L. Receptive field organization determines pyramidal cell stimulus-encoding capability and spatial stimulus selectivity. J Neurosci. 2002; 22:4577–4590. [PubMed: 12040065]

Bastian J, Chacron MJ, Maler L. Plastic and non-plastic cells perform unique roles in a network capable of adaptive redundancy reduction. Neuron. 2004; 41:767–779. [PubMed: 15003176]

Bastian J, Electrolocation I. How the electroreceptors of *Apteronotus albifrons* code for moving objects and other electrical stimuli. J Comp Physiol [A]. 1981; 144:465–479.

Bastian J, Nguyenkim J. Dendritic modulation of burst-like firing in sensory neurons. J Neurophysiol. 2001; 85:10–22. [PubMed: 11152701]

Benda J, Herz AV. A universal model for spike-frequency adaptation. Neural Comput. 2003; 15:2523–2564. [PubMed: 14577853]

Berman N, Dunn RJ, Maler L. Function of NMDA receptors and persistent sodium channels in a feedback pathway of the electrosensory system. J Neurophysiol. 2001; 86:1612–1621. [PubMed: 11600624]

Berman NJ, Hincke MT, Maler L. Inositol 1,4,5-trisphosphate receptor localization in the brain of a weakly electric fish (*Apteronotus leptorhynchus*) with emphasis on the electrosensory system. J Comp Neurol. 1995; 361:512–524. [PubMed: 8550896]

Berman NJ, Maler L. Distal versus proximal inhibitory shaping of feedback excitation in the electrosensory lateral line lobe: implications for sensory filtering. J Neurophysiol. 1998a; 80:3214–3232. [PubMed: 9862917]

Berman NJ, Maler L. Inhibition evoked from primary afferents in the electrosensory lateral line lobe of the weakly electric fish (*Apteronotus leptorhynchus*). J Neurophysiol. 1998b; 80:3173–3196. [PubMed: 9862915]

Berman NJ, Maler L. Interaction of $GABA_B$-mediated inhibition with voltage-gated currents of pyramidal cells: computational mechanism of a sensory searchlight. J Neurophysiol. 1998c; 80:3197–3213. [PubMed: 9862916]

Bond CT, Maylie J, Adelman JP. Small-conductance calcium-activated potassium channels. Ann NY Acad Sci. 1999; 868:370–378. [PubMed: 10414306]

Bond CT, Maylie J, Adelman JP. SK channels in excitability, pacemaking and synaptic integration. Curr Opin Neurobiol. 2005; 15:305–311. [PubMed: 15922588]

Borst A, Haag J. Effects of mean firing on neural information rate. J Comput Neurosci. 2001; 10:213–221. [PubMed: 11361260]

Borst A, Theunissen FE. Information theory and neural coding. Nat Neurosci. 1999; 2:947–957. [PubMed: 10526332]

Bottai D, Dunn RJ, Ellis W, Maler L. N-methyl-D-aspartate receptor 1 mRNA distribution in the central nervous system of the weakly electric fish Apteronotus leptorhynchus. J Comp Neurol. 1997; 389:65–80. [PubMed: 9390760]

Brumberg JC, Nowak LG, McCormick DA. Ionic mechanisms underlying repetitive high-frequency burst firing in supragranular cortical neurons. J Neurosci. 2000; 20:4829–4843. [PubMed: 10864940]

Chacron MJ. Nonlinear information processing in a model sensory system. J Neurophysiol. 2006; 95:2933–2946. [PubMed: 16495358]

Chacron MJ, Bastian J. Population coding by electrosensory neurons. J Neurophysiol. 2008; 99:1825–1835. [PubMed: 18256161]

Chacron MJ, Doiron B, Maler L, Longtin A, Bastian J. Non-classical receptive field mediates switch in a sensory neuron's frequency tuning. Nature. 2003a; 423:77–81. [PubMed: 12721628]

Chacron MJ, Lindner B, Longtin A. Threshold fatigue and information transfer. J Comput Neurosci. 2007; 23:301–311. [PubMed: 17436067]

Chacron MJ, Longtin A, Maler L. Negative interspike interval correlations increase the neuronal capacity for encoding time-varying stimuli. J Neurosci. 2001a; 21:5328–5343. [PubMed: 11438609]

Chacron MJ, Longtin A, Maler L. Simple models of bursting and non-bursting electroreceptors. Neurocomputing. 2001b; 38:129–139.

Chacron MJ, Longtin A, Maler L. The effects of spontaneous activity, background noise, and the stimulus ensemble on information transfer in neurons. Netw Comput Neural Syst. 2003b; 14:803–824.

Chacron MJ, Longtin A, Maler L. To burst or not to burst? J Comput Neurosci. 2004; 17:127–136. [PubMed: 15306735]

Chacron MJ, Longtin A, Maler L. Delayed excitatory and inhibitory feedback shape neural information transmission. Phys Rev E. 2005a; 72:051917.

Chacron MJ, Maler L, Bastian J. Electroreceptor neuron dynamics shape information transmission. Nat Neurosci. 2005b; 8:673–678. [PubMed: 15806098]

Chacron MJ, Maler L, Bastian J. Feedback and feedforward control of frequency tuning to naturalistic stimuli. J Neurosci. 2005c; 25:5521–5532. [PubMed: 15944380]

Dayan, P., Abbott, LF. Theoretical Neuroscience: Computational and Mathematical Modeling of Neural Systems. Cambridge, MA: MIT; 2001.

Destexhe A, Paré D. Impact of network activity on the integrative properties of neocortical pyramidal neurons in vivo. J Neurophysiol. 1999; 81:1531–1547. [PubMed: 10200189]

Doiron B, Chacron MJ, Maler L, Longtin A, Bastian J. Inhibitory feedback required for network oscillatory responses to communication but not prey stimuli. Nature. 2003a; 421:539–543. [PubMed: 12556894]

Doiron B, Laing C, Longtin A, Maler L. Ghostbursting: a novel neuronal burst mechanism. J Comput Neurosci. 2002; 12:5–25. [PubMed: 11932557]

Doiron B, Longtin A, Berman N, Maler L. Subtractive and divisive inhibition: effect of voltage-dependent inhibitory conductances and noise. Neural Comput. 2001a; 13:227–248. [PubMed: 11177434]

Doiron B, Longtin A, Turner RW, Maler L. Model of gamma frequency burst discharge generated by conditional backpropagation. J Neurophysiol. 2001b; 86:1523–1545. [PubMed: 11600618]

Doiron B, Noonan L, Lemon N, Turner RW. Persistent Na^+ current modifies burst discharge by regulating conditional backpropagation of dendritic spikes. J Neurophysiol. 2003b; 89:324–337. [PubMed: 12522183]

Doiron B, Oswald AM, Maler L. Interval coding. II. Dendrite-dependent mechanisms. J Neurophysiol. 2007; 97:2744–2757. [PubMed: 17409177]

Dunn RJ, Bottai D, Maler L. Molecular biology of the apteronotus NMDA receptor NR1 subunit. J Exp Biol. 1999; 202:1319–1326. [PubMed: 10210672]

Ellis LD, Krahe R, Bourque CW, Dunn RJ, Chacron MJ. Muscarinic receptors control frequency tuning through the downregulation of an A-type potassium current. J Neurophysiol. 2007a; 98:1526–1537. [PubMed: 17615127]

Ellis LD, Maler L, Dunn RJ. Differential distribution of SK channel subtypes in the brain of the weakly electric fish Apteronotus leptorhynchus. J Comp Neurol. 2008; 507:1964–1978. [PubMed: 18273887]

Ellis LD, Mehaffey WH, Harvey-Girard E, Turner RW, Maler L, Dunn RJ. SK channels provide a novel mechanism for the control of frequency tuning in electrosensory neurons. J Neurosci. 2007b; 27:9491–9502. [PubMed: 17728462]

Faber ES, Delaney AJ, Sah P. SK channels regulate excitatory synaptic transmission and plasticity in the lateral amygdala. Nat Neurosci. 2005; 8:635–641. [PubMed: 15852010]

Faber ES, Sah P. Functions of SK channels in central neurons. Clin Exp Pharmacol Physiol. 2007; 34:1077–1083. [PubMed: 17714097]

Frank, K., Becker, MC. Physical Techniques in Biological Research. New York: Academic; 1964. Microelectrodes for recording and stimulation; p. 23-84.

Gabbiani F, Metzner W, Wessel R, Koch C. From stimulus encoding to feature extraction in weakly electric fish. Nature. 1996; 384:564–567. [PubMed: 8955269]

Garaschuk O, Schneggenburger R, Schirra C, Tempia F, Konnerth A. Fractional Ca^{2+} currents through somatic and dendritic glutamate receptor channels of rat hippocampal CA1 pyramidal neurones. J Physiol. 1996; 491:757–772. [PubMed: 8815209]

Glitsch MD. Calcium influx through N-methyl-D-aspartate receptors triggers GABA release at interneuron-Purkinje cell synapse in rat cerebellum. Neuroscience. 2008; 151:403–409. [PubMed: 18055124]

Gonon FG. Nonlinear relationship between impulse flow and dopamine released by rat midbrain dopaminergic neurons as studied by in vivo electrochemistry. Neuroscience. 1988; 24:19–28. [PubMed: 3368048]

Harvey-Girard E, Dunn RJ. Excitatory amino acid receptors of the electrosensory system: the NR1/NR2B N-methyl-D-aspartate receptor. J Neurophysiol. 2003; 89:822–832. [PubMed: 12574460]

Hausser M, Mel B. Dendrites: bug or feature? Curr Opin Neurobiol. 2003; 13:372–383. [PubMed: 12850223]

Hines ML, Carnevale NT. The NEURON simulation environment. Neural Comput. 1997; 9:1179–1209. [PubMed: 9248061]

Izhikevich EM. Neural excitability, spiking, and bursting. Int J Bifurcations Chaos. 2000; 10:1171–1269.

Johnson SW, Wu YN. Multiple mechanisms underlie burst firing in rat midbrain dopamine neurons in vitro. Brain Res. 2004; 1019:293–296. [PubMed: 15306267]

Jung H-Y, Staff NP, Spruston N. Action potential bursting in subicular pyramidal neurons is driven by a calcium tail current. J Neurosci. 2001; 21:3312–3321. [PubMed: 11331360]

Kepecs A, Lisman J. Information encoding and computation with spikes and bursts. Netw Comput Neural Syst. 2003; 14:103–118.

Kepecs A, Wang XJ, Lisman J. Bursting neurons signal input slope. J Neurosci. 2002; 22:9053–9062. [PubMed: 12388612]

Kim U, McCormick DA. The functional influence of burst and tonic firing mode on synaptic interactions in the thalamus. J Neurosci. 1998; 18:9500–9516. [PubMed: 9801387]

Koh DS, Geiger JR, Jonas P, Sakmann B. Ca(2+)-permeable AMPA and NMDA receptor channels in basket cells of rat hippocampal dentate gyrus. J Physiol. 1995; 485:383–402. [PubMed: 7545230]

Kohler M, Hirschberg B, Bond CT, Kinzie JM, Marrion NV, Maylie J, Adelman JP. Small-conductance, calcium-activated potassium channels from mammalian brain. Science. 1996; 273:1709–1714. [PubMed: 8781233]

Krahe R, Bastian J, Chacron MJ. Temporal processing across multiple topographic maps in the electrosensory system. J Neurophysiol. 2008; 100:852–867. [PubMed: 18509073]

Krahe R, Gabbiani F. Burst firing in sensory systems. Nat Rev Neurosci. 2004; 5:13–23. [PubMed: 14661065]

Laing CR, Doiron B, Longtin A, Noonan L, Turner RW, Maler L. Type I burst excitability. J Comput Neurosci. 2003; 14:329–342. [PubMed: 12766431]

Lemon N, Turner RW. Conditional spike backpropagation generates burst discharge in a sensory neuron. J Neurophysiol. 2000; 84:1519–1530. [PubMed: 10980024]

Lesica NA, Stanley GB. Encoding of natural scene movies by tonic and burst spikes in the lateral geniculate nucleus. J Neurosci. 2004; 24:10731–10740. [PubMed: 15564591]

Lisman JE. Bursts as a unit of neural information: making unreliable synapses reliable. Trends Neurosci. 1997; 20:38–43. [PubMed: 9004418]

Llinas RR, Steriade M. Bursting of thalamic neurons and states of vigilance. J Neurophysiol. 2006; 95:3297–3308. [PubMed: 16554502]

London M, Hausser M. Dendritic computation. Annu Rev Neurosci. 2005; 28:503–532. [PubMed: 16033324]

MacDermott AB, Mayer ML, Westbrook GL, Smith SJ, Barker JL. NMDA-receptor activation increases cytoplasmic calcium concentration in cultured spinal cord neurones. Nature. 1986; 321:519–522. [PubMed: 3012362]

Maler L. The posterior lateral line lobe of certain gymnotiform fish. Quantitative light microscopy. J Comp Neurol. 1979; 183:323–363. [PubMed: 762262]

Maler L, Sas E, Johnston S, Ellis W. An atlas of the brain of the weakly electric fish *Apteronotus Leptorhynchus*. J Chem Neuroanat. 1991; 4:1–38. [PubMed: 2012682]

Mayer ML, Westbrook GL. Permeation and block of N-methyl-D-aspartic acid receptor channels by divalent cations in mouse cultured central neurones. J Physiol. 1987; 394:501–527. [PubMed: 2451020]

Mehaffey WH, Ellis LD, Krahe R, Dunn RJ, Chacron MJ. Ionic and neuromodulatory regulation of burst discharge controls frequency tuning. J Physiol. 2008a; 102:195–208.

Mehaffey WH, Maler L, Turner RW. Intrinsic frequency tuning in ELL pyramidal cells varies across electrosensory maps. J Neurophysiol. 2008b; 99:2641–2655. [PubMed: 18367702]

Metzner W, Koch C, Wessel R, Gabbiani F. Feature extraction by burst-like spike patterns in multiple sensory maps. J Neurosci. 1998; 18:2283–2300. [PubMed: 9482813]

Ngo-Anh TJ, Bloodgood BL, Lin M, Sabatini BL, Maylie J, Adelman JP. SK channels and NMDA receptors form a Ca^{2+}-mediated feedback loop in dendritic spines. Nat Neurosci. 2005; 8:642–649. [PubMed: 15852011]

Noonan L, Doiron B, Laing C, Longtin A, Turner RW. A dynamic dendritic refractory period regulates burst discharge in the electrosensory lobe of weakly electric fish. J Neurosci. 2003; 23:1524–1534. [PubMed: 12598641]

Nowak L, Bregestovski P, Ascher P, Herbet A, Prochiantz A. Magnesium gates glutamate-activated channels in mouse central neurones. Nature. 1984; 307:462–465. [PubMed: 6320006]

Oswald AM, Doiron B, Maler L. Interval coding. I. Burst interspike intervals as indicators of stimulus intensity. J Neurophysiol. 2007; 97:2731–2743. [PubMed: 17409176]

Oswald AMM, Chacron MJ, Doiron B, Bastian J, Maler L. Parallel processing of sensory input by bursts and isolated spikes. J Neurosci. 2004; 24:4351–4362. [PubMed: 15128849]

Ping HX, Shepard PD. Apamin-sensitive Ca(2+)-activated K^+ channels regulate pacemaker activity in nigral dopamine neurons. Neuroreport. 1996; 7:809–814. [PubMed: 8733751]

Ramcharan EJ, Gnadt JW, Sherman SM. Burst and tonic firing in thalamic cells of unanesthetized, behaving monkeys. Vis Neurosci. 2000; 17:55–62. [PubMed: 10750826]

Reynolds IJ, Miller RJ. Allosteric modulation of N-methyl-D-aspartate receptors. Adv Pharmacol. 1990; 21:101–126. [PubMed: 2148268]

Ritz R, Sejnowski TJ. Synchronous oscillatory activity in sensory systems: new vistas on mechanisms. Curr Opin Neurobiol. 1997; 7:536–546. [PubMed: 9287205]

Sadeghi SG, Chacron MJ, Taylor MC, Cullen KE. Neural variability, detection thresholds, and information transmission in the vestibular system. J Neurosci. 2007; 27:771–781. [PubMed: 17251416]

Sah P. Ca 2+-activated K^+ currents in neurones: types, physiological roles and modulation. Trends Neurosci. 1996; 19:150–154. [PubMed: 8658599]

Sah P, Faber ES. Channels underlying neuronal calcium-activated potassium currents. Prog Neurobiol. 2002; 66:345–353. [PubMed: 12015199]

Saunders J, Bastian J. The physiology and morphology of two classes of electrosensory neurons in the weakly electric fish *Apteronotus leptorhynchus*. J Comp Physiol A. 1984; 154:199–209.

Sherman SM. Tonic and burst firing: dual modes of thalamocortical relay. Trends Neurosci. 2001; 24:122–126. [PubMed: 11164943]

Sherman SM, Guillery RW. The role of the thalamus in the flow of information to the cortex. Philos Trans R Soc Lond B Biol Sci. 2002; 357:1695–1708. [PubMed: 12626004]

Steriade M. Impact of network activities on neuronal properties in corticothalamic systems. J Neurophysiol. 2001; 86:1–39. [PubMed: 11431485]

Swensen AM, Bean BP. Ionic mechanisms of burst firing in dissociated Purkinje neurons. J Neurosci. 2003; 23:9650–9663. [PubMed: 14573545]

Turner RW, Maler L. Oscillatory and burst discharge in the apteronotid electrosensory lateral line lobe. J Exp Biol. 1999; 202:1255–1265. [PubMed: 10210666]

Turner RW, Maler L, Burrows M. Electroreception and electrocommunication. J Exp Biol. 1999; 202:1167–1458. [PubMed: 10210659]

Turner RW, Maler L, Deerinck T, Levinson SR, Ellisman MH. TTX-sensitive dendritic sodium channels underlie oscillatory discharge in a vertebrate sensory neuron. J Neurosci. 1994; 14:6453–6471. [PubMed: 7965050]

Vergara C, Latorre R, Marrion NV, Adelman JP. Calcium-activated potassium channels. Curr Opin Neurobiol. 1998; 8:321–329. [PubMed: 9687354]

Wagner J, Keizer J. Effects of rapid buffers on Ca^{2+} diffusion and Ca^{2+} oscillations. Biophys J. 1994; 67:447–456. [PubMed: 7919018]

Wang, XJ., Rinzel, J. Oscillatory and bursting properties of neurons. In: Arbib, MA., editor. The Handbook of Brain Theory and Neural Networks. Cambridge, MA: MIT Press; 1995. p. 686-691.

Wolfart J, Debay D, Le Masson G, Destexhe A, Bal T. Synaptic background activity controls spike transfer from thalamus to cortex. Nat Neurosci. 2005; 8:1760–1767. [PubMed: 16261132]

Zakon HH, Oestreich J, Tallarovic S, Triefenbach F. EOD modulations of brown ghost electric fish: JARs, chirps, rises, and dips. J Physiol Paris. 2002; 96:451–458. [PubMed: 14692493]

Zupanc GKH, Airey JA, Maler L, Sutko JL, Ellisman MH. Immunohistochemical localization of ryanodine binding protein in the central nervous system of gymnotiform fish. J Comp Neurol. 1992; 325:135–151. [PubMed: 1460110]

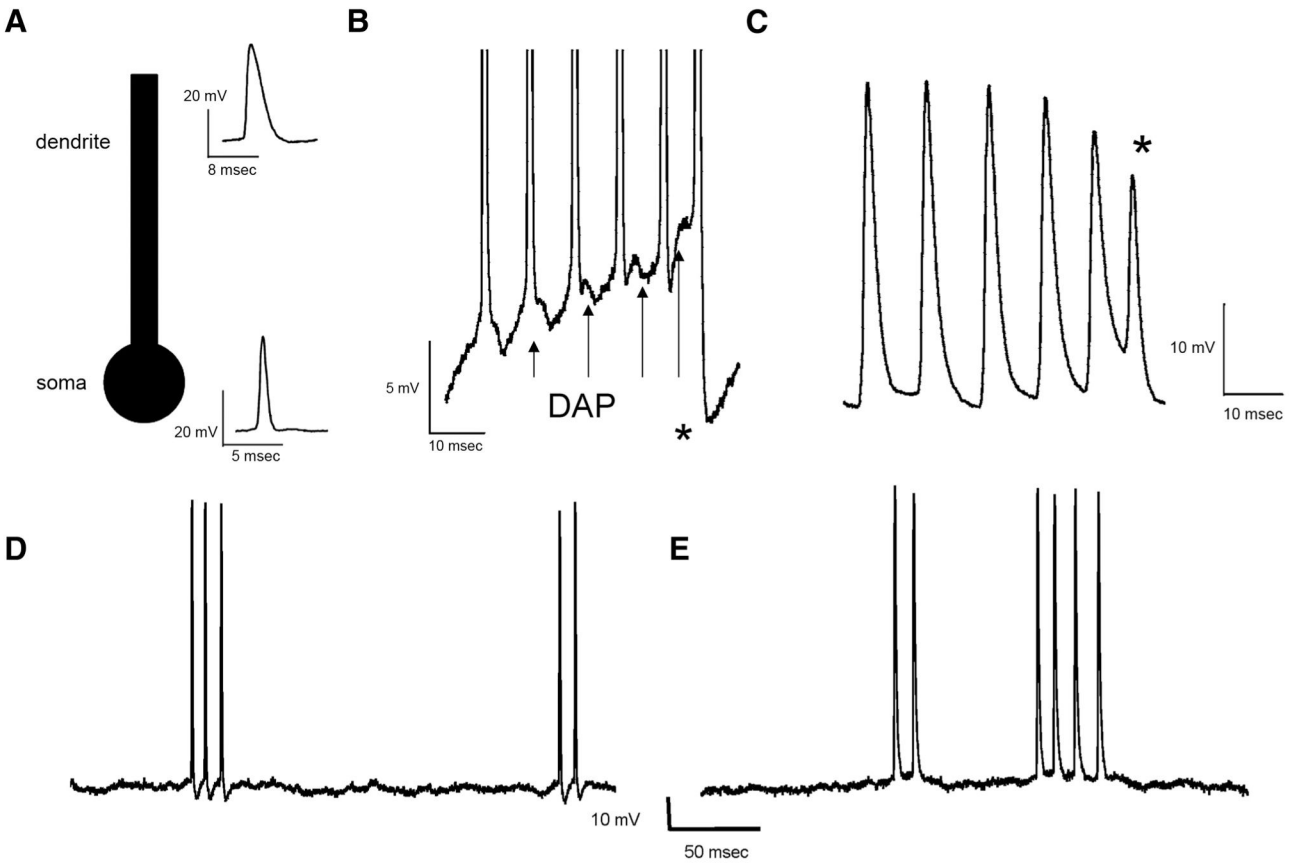

FIG. 1.

Differences between bursting in vivo and in vitro. *A*: schematic representation of the somatic and dendritic compartments that are necessary for bursting seen in vitro. *Insets*: a dendritic action potential (*top*) and somatic action potential (*bottom*). *B*: somatic in vitro recording from a pyramidal cell showing the ramp depolarization during the burst, the depolarizing afterpotential (DAP) growth (arrows), and the shortening of the interspike interval. The burst terminates with a burst afterhyperpolarization (bAHP, asterisk). *C*: dendritic in vitro recording from a pyramidal cell showing the decrease in spike height throughout the burst that is terminated by a dendritic failure (asterisk) when the interspike interval falls below the dendritic refractory period. *D* and *E*: example in vivo recordings from pyramidal cells. Based on spike shape, *D* resembles an in vitro somatic recording, whereas *E* resembles an in vitro dendritic recording. However, we found no evidence for depolarizing ramps, bAHPs, dendritic failures, or a decrease in spike height during the burst.

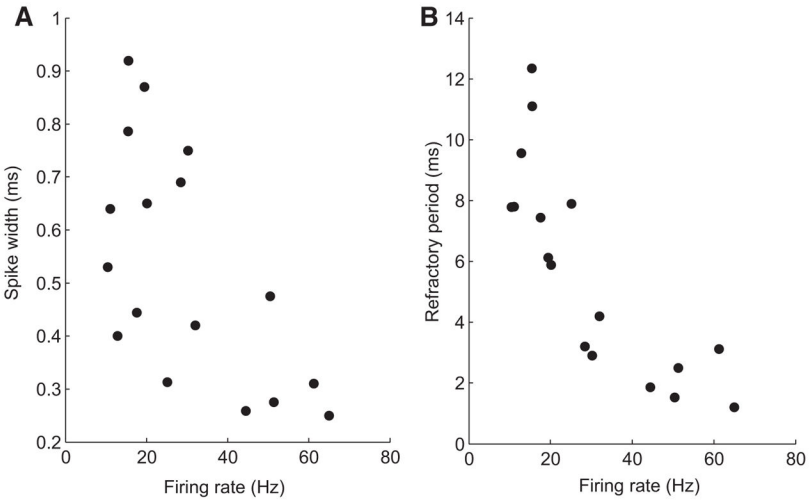

FIG. 2.

Influence of pyramidal cell firing rate on firing properties. *A*: the spike width (full width at half-maximum) was negatively correlated with firing rate but still within the range observed in vitro. *B*: the refractory period was also negatively correlated with firing rate but was significantly higher than what is typically observed in vitro.

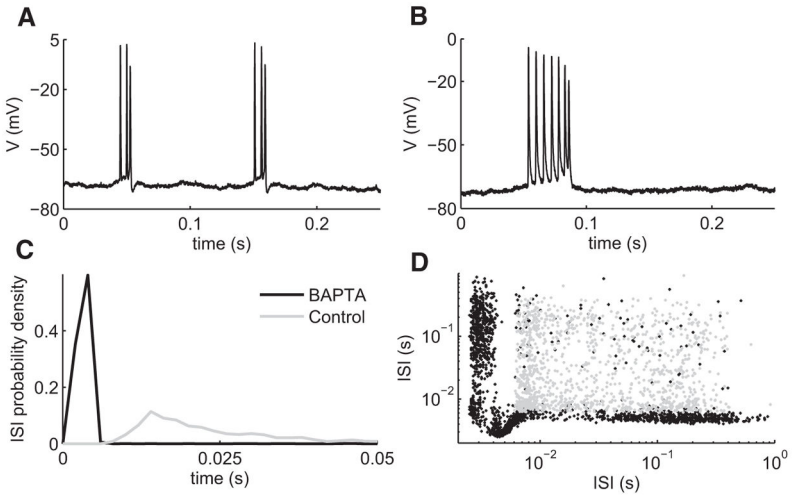

FIG. 3.

The Ca^{2+} chelator BAPTA induces in vitro–like burst firing in vivo. *A*: recording from the same cell as Fig. 1*D* after BAPTA treatment showing ramp depolarizations (*inset*) and bAHPs after each burst. *B*: recording from the same cell as Fig. 1*E* showing a decrease in spike height during the burst that is terminated with a dendritic failure. *C*: interspike interval (ISI) distribution under control (gray) and after BAPTA treatment (black) showing a decrease in the cell's absolute refractory period. *D*: ISI return map under control (gray) and after BAPTA treatment (black) showing a transition to a bursting regime.

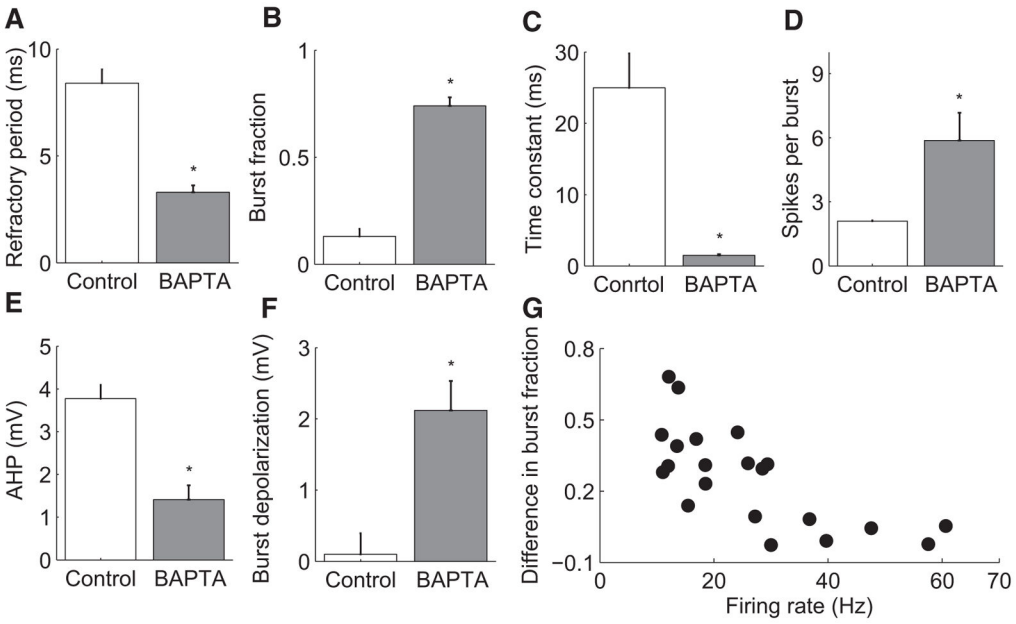

FIG. 4.

BAPTA affects electrosensory lateral line lobe (ELL) pyramidal cell firing properties in vivo. Asterisk indicates significant difference ($P < 0.05$). *A*: BAPTA decreases the cell's refractory period. *B*: BAPTA increases burst fraction (i.e., fraction of ISIs <10 ms). *C*: BAPTA significantly decreases the time constant obtained by fitting an exponential to the decaying part of the ISI distribution. *D*: BAPTA significantly increases the number of spikes per burst. *E*: BAPTA significantly decreases the AHP. *F*: BAPTA induces a depolarization during bursting. *G*: the effects of BAPTA were different for cells of different morphologies. BAPTA tended to have the greatest effect in cells that had low firing rates as shown by a significant negative correlation between the change in burst fraction induced by BAPTA and the cell's mean firing rate under control conditions. The asterisks indicate statistical significance at the $P = 0.05$ level.

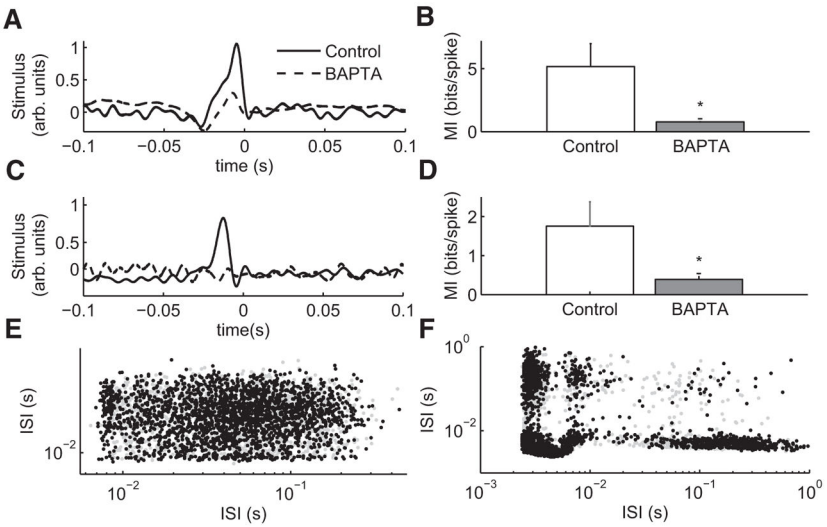

FIG. 5.

BAPTA significantly affects pyramidal cell responses to sensory input. *A*: representative spike triggered averages for global noise stimulation for control (dashed) and BAPTA (black) conditions. In both cases, the action potential occurs at *time 0*. *B*: BAPTA significantly reduces the mutual information rate for global stimulation. *C*: representative spike triggered average for local noise stimulation for control (dashed) and BAPTA (black) conditions. In both cases, the action potential occurs at *time 0*. *D*: BAPTA also significantly reduces the mutual information rate for local stimulation. *E*: ISI return map under control conditions for baseline (gray) and stimulated (black) activity. Note that both maps are quite different as can be seen by the relative lack of overlap between points. *F*: ISI return map after treatment with BAPTA for baseline (gray) and stimulated (black) conditions. Note the large overlap between both conditions indicating that the activity is quite similar under both baseline and stimulated conditions, thereby implying that the stimulus has very little effect on the neural activity as seen by the spike triggered average. The asterisks indicate statistical significance at the $P = 0.05$ level.

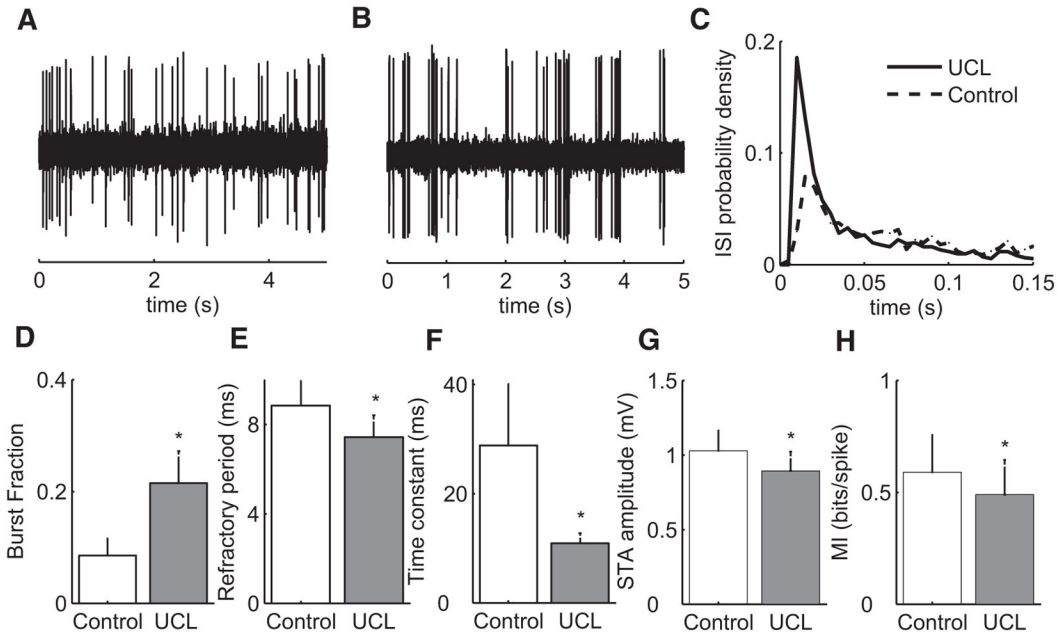

FIG. 6.

The small conductance (SK) channel blocker, UCL-1684 (UCL), induces burst firing with characteristics similar to those observed under BAPTA treatment. *A*: representative extracellular recording under control conditions. *B*: extracellular recording from the same neuron after UCL treatment showing burst firing. *C*: ISI distributions under control (dotted) and after UCL treatment (black). *D*: UCL significantly increases the burst fraction. *E*: UCL significantly decreases the cell's absolute refractory period. *E*: UCL significantly decreases the time constant. Note that the changes seen in *C–F* are similar to the changes seen with BAPTA (cf. with Fig. 4). *G*: like BAPTA, UCL causes a significant reduction in the spike-triggered average amplitude. *H*: like BAPTA, UCL also causes a significant reduction in the mutual information rate *MI*. The asterisks indicate statistical significance at the $P = 0.05$ level.

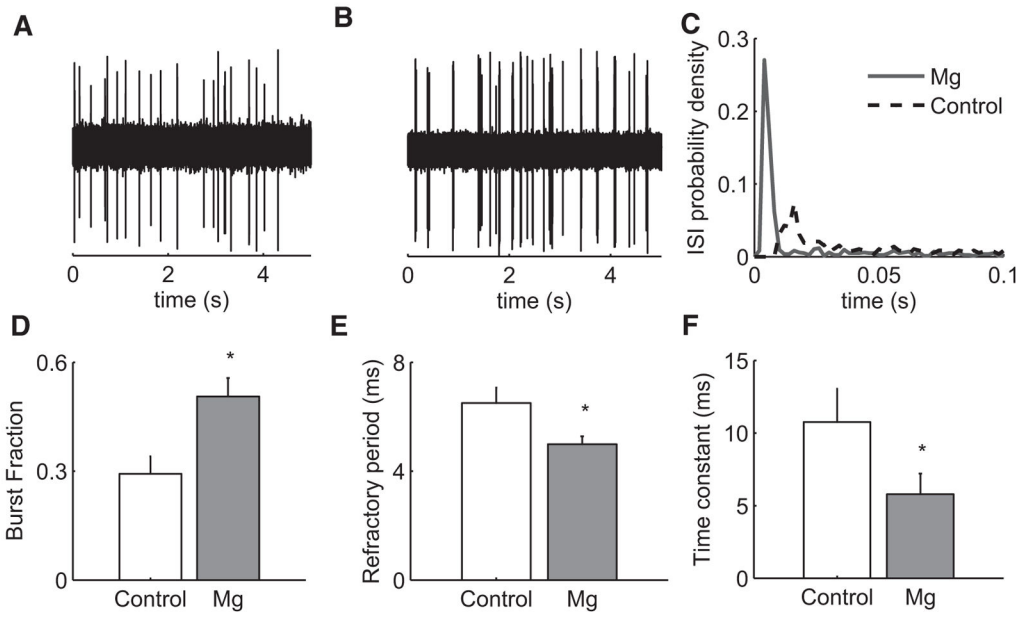

FIG. 7.

The *N*-methyl-D-aspartate (NMDA) channel blocker, Mg^{2+}, induces burst firing in pyramidal cells with characteristics similar to those seen with BAPTA and UCL. *A*: representative extracellular recording under control conditions. *B*: extracellular recording from the same neuron after Mg^{2+} treatment showing burst firing. *C*: ISI distributions under control (dotted) and after Mg^{2+} treatment (black). *D*: Mg^{2+} significantly increases the burst fraction. *E*: Mg^{2+} significantly decreases the cell's absolute refractory period. *E*: Mg^{2+} significantly decreases the time constant. Note that the changes seen in *C*–*F* are similar to the changes seen with BAPTA and UCL (cf. with Figs. 4 and 7, respectively). The asterisks indicate statistical significance at the $P = 0.05$ level.

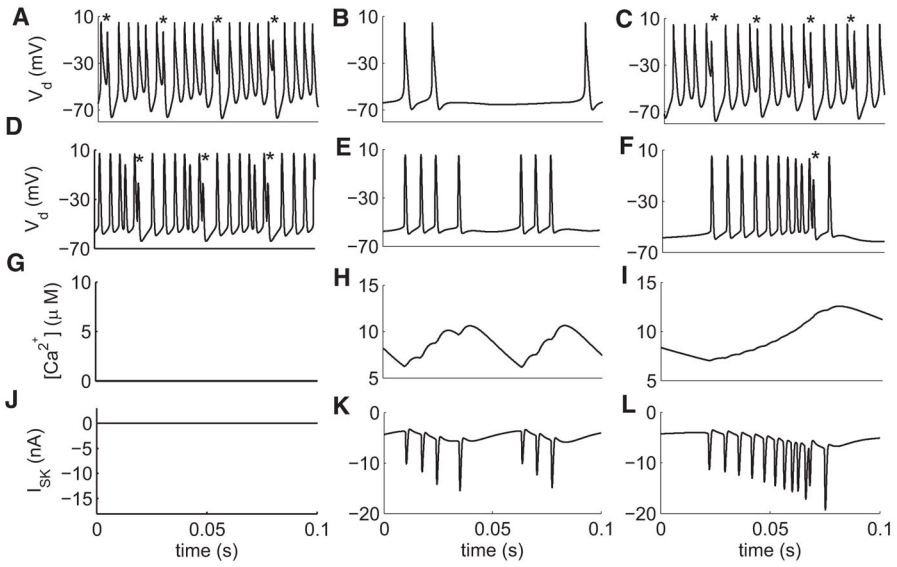

FIG. 8.

Modeling the differences between bursting seen in vitro and bursting seen in vivo. *A*: simulation of a large multicompartmental model of an ELL pyramidal cell with partially blocked SK current (i.e., g_{SK} = 2.06 μS) produces burst firing with dendritic failures (asterisk). *B*: increasing SK current (g_{SK} = 7× 10^{-5} μS, f_{Ca} = 0.03/ms) counteracts the DAP and does not lead to dendritic failure in the dendritic membrane potential. *C*: increasing the calcium time constant (i.e., setting f_{Ca} = 0.0008/ms) in the model reproduces the effects of BAPTA. Dendritic failures are seen in the dendritic membrane potential (asterisks). *D*: simulation of the reduced 2-compartmental model without an NMDA current (i.e., g_{nmda} = 0) produced burst firing that was qualitatively similar to that seen with the large model with dendritic failures (asterisk). *E*: addition of the NMDA current (g_{nmda} = 20 mS/cm^2, f_{Ca} = 0.03/ms) counteracts the DAP and does not lead to dendritic failure in the dendritic membrane potential. *F*: increasing the calcium time constant (i.e., setting f_{Ca} = 0.008/ms) in the model reproduces the effects of BAPTA. Dendritic failures are seen in the dendritic membrane potential (asterisk). *G*: Ca^{2+} concentration as a function of time in the reduced model with g_{nmda} = 0. *H*: setting g_{nmda} = 20 mS/cm^2, f_{Ca} = 0.03/ms causes accumulation of calcium during repetitive firing. The calcium concentration decreases during periods of silence. Note that the cumulative increase in the current is mostly because of the depolarization throughout the burst (*E*) that is caused by the DAP growth and not because of the conductance that saturates well before 10 μM. *I*: setting f_{Ca} = 0.008/ms causes a slower accumulation of calcium during repetitive firing. *J*: SK current as a function of time for g_{nmda} = 0. *K*: setting g_{nmda} = 20 mS/cm^2, f_{Ca} = 0.03/ms causes a rapid accumulation of calcium during repetitive firing that causes cumulative activation of the SK current, which leads to early burst termination. *L*: setting f_{Ca} = 0.008/ms causes a slower cumulative activation of the SK current, which is not enough to prevent burst termination by a dendritic failure.

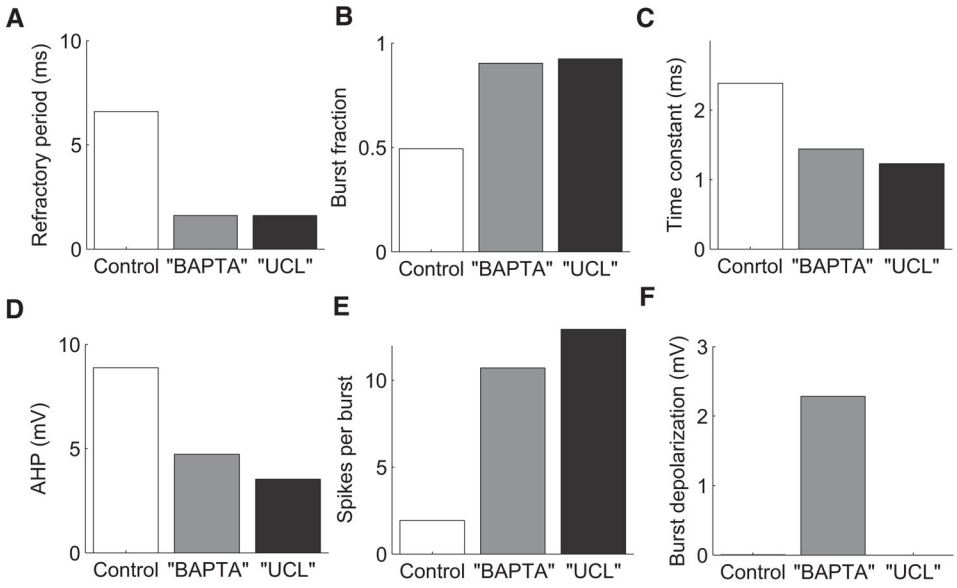

FIG. 9.

Changing the calcium time constant in the model induces changes in the firing properties that are similar to those seen with BAPTA in vivo. *A*: the refractory period is less under simulated BAPTA and UCL conditions. *B*: the burst fraction is greater under simulated BAPTA and UCL conditions. *C*: the time constant is less under BAPTA and UCL conditions. *D*: the AHP is less under simulated BAPTA and UCL conditions. *E*: the number of spikes per burst is greater under simulated BAPTA and UCL conditions. *F*: the depolarization during the burst is greater under simulated BAPTA and UCL conditions.

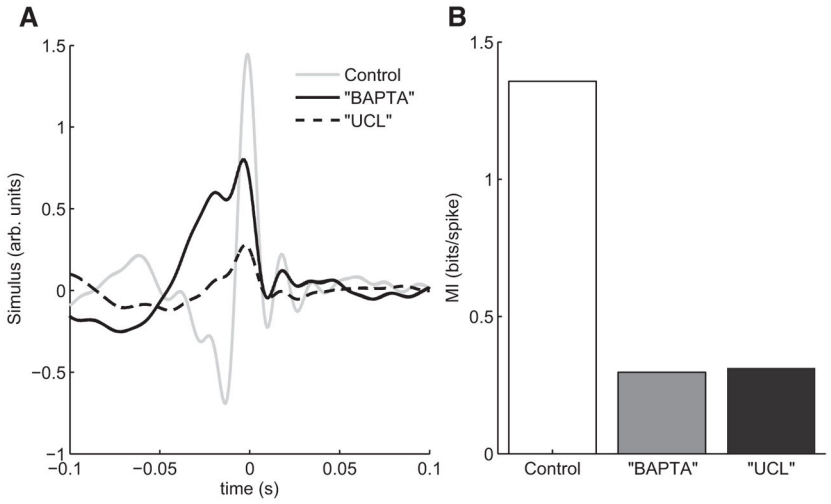

FIG. 10.

The model shows a weaker response to noise current injection when we increase f_{Ca} from 0.003 (control) to 0.008/ms (BAPTA) and decrease g_{SK} from 7 to 4 mS/cm^2 (UCL). *A*: spike triggered averages under simulated control (gray), BAPTA (black), and UCL (dashed) conditions. *B*: the mutual information rate is greater under simulated control conditions than for either simulated BAPTA or UCL conditions.